Physica Medica 66 (2019) 97–103

Contents lists available at ScienceDirect

Physica Medica

journal homepage: www.elsevier.com/locate/ejmp

Original paper

New calculation method for 3D dose distribution in tetrahedral-mesh phantoms in Geant4

Min Cheol Han[a], Youngmo Ku[b], Hyun Su Lee[b], Yeon Soo Yeom[c], Haegin Han[b], Chan Hyeong Kim[b,*]

[a] Department of Radiation Oncology, Yonsei University College of Medicine, Seoul 03722, South Korea
[b] Department of Nuclear Engineering, Hanyang University, Seoul 04763, South Korea
[c] Division of Cancer Epidemiology & Genetics, National Cancer Institute, MD 20892-9760, USA

ARTICLE INFO

Keywords:
Tetrahedral-mesh
Computational phantom
3D dose distribution
Monte Carlo
Geant4

ABSTRACT

The tetrahedral-mesh (TM) geometry, which is a very promising geometry for computational human phantoms, has a limitation in 3D dose distribution calculation for medical applications. Even though Geant4 provides the read-out geometry for calculating 3D dose distribution in the TM geometry, this method significantly slows down the computation speed. In the present study, we developed a new method, called Moving Voxel-based Dose-Distribution Calculator (MVDDC), to rapidly calculate a 3D dose distribution in a TM geometry. To evaluate the performance of the MVDDC method, a simple TM cubic phantom and a human phantom were implemented in Geant4. Subsequently, the phantoms were irradiated with proton spot beams under various conditions, and the obtained results were compared with those of the read-out geometry method. The results show that there is no significant difference between the dose distributions calculated using the new method and the read-out geometry method. With respect to the computational performance, the speeds of simulations using the MVDDC were approximately 1.4–2.7 times faster than those of the simulations using the read-out geometry method.

1. Introduction

Computational human phantoms (CHPs) are widely used in diagnostic and therapeutic medical applications for calculating dose distribution in Monte Carlo codes [1–3]. The CHPs have been developed over time in order to realize a more realistic and accurate representation of the human body. Since the 1980s, voxel phantoms, which are constructed based on computational tomography (CT) or magnetic resonance (MR) images of the human body, have been used to obtain realistic anatomy of the human body. Nevertheless, the voxel phantoms have limitations in representing the human anatomy. For instance, the voxel phantoms cannot properly model thin/small or very complicated structures (e.g., skin, arteries, and atheroma) owing to the nature of voxel geometry [4,5] and the voxel geometry is not deformable. From a medical point of view, fine structures obtained from other imaging modalities (e.g., spinal cord, atheroma, etc.) or detailed implementation structures modeled from computer-assisted design (CAD) (e.g., brachytherapy seeds, artificial implants, hip replacements, screws, etc.) cannot implemented in voxel geometry directly [5]. To overcome the limitations, several investigators [4,6–9] developed mesh-type CHPs using non-uniform rational B-spline (NURBS), polygonal mesh (PM), and tetrahedral mesh (TM) geometries. These new types of phantoms allow for the modeling of thin/small and complex organ/tissue structures with smooth surfaces (e.g., breast skin and tumors [10–13], eye [14], and small bowel [15]). Currently, NURBS phantoms cannot be used in Monte Carlo codes; only PM and TM phantoms can be directly used. In particular, the TM phantoms provide a much faster simulation speed than the PM phantoms [9]. The TM geometry can also model heterogeneous density distribution in an organ/tissue using their tetrahedral-mesh structure. For these advantages, recently the International Commission on Radiological Protection (ICRP) has decided to complement the voxel reference phantoms by realizing them also in TM geometry [16].

The TM geometry, however, has a fundamental limitation that does not apply to voxel geometry: it is not possible to calculate a detailed 3D dose distribution for medical applications. Note that in a voxel geometry, a 3D dose distribution can be directly calculated using the structure of the voxel geometry. In Geant4 [17–19], a detailed 3D dose distribution in the TM geometry can be calculated by using a read-out geometry method. The read-out geometry is a virtual/parallel geometry and enables us to collect particle information corresponding to the readout segmentation [20]; nevertheless, the use of the read-out

* Corresponding author.
E-mail address: chkim@hanyang.ac.kr (C.H. Kim).

https://doi.org/10.1016/j.ejmp.2019.09.239
Received 17 July 2019; Received in revised form 27 August 2019; Accepted 23 September 2019
Available online 01 October 2019

geometry method significantly slows down the computation speed due to the requirement of an additional dedicated-navigator for the read-out geometry. For a fast calculation of dose distribution without using the read-out geometry method, Sarrut et al. [21] alternatively proposed a random indexing method, which determines the scoring index of a continuously deposited energy occurred by charged particle from a randomly selected point between two endpoints of a step (i.e., PreStepPoint and PostStepPoint). However, this method tends to require a much larger number of primary particles to achieve the same statistical significance as the read-out geometry method.

In the present study, a new method called the moving voxel-based dose-distribution calculation (MVDDC) was developed to rapidly calculate the dose distribution in a TM geometry, without using the read-out geometry method in Geant4. The performance of the method was then evaluated by comparing the calculated dose distribution and computational speed with those obtained using the read-out geometry method.

2. Material and methods

2.1. Basic concept of read-out geometry method

The read-out geometry is a virtual geometry which can be defined in parallel to any complicated geometries in the real world. Using the read-out geometry, it is possible to define scoring volume boundaries corresponding to the detector array that allows Geant4 to accumulate particle tracking information (e.g., continuously deposited energy during a step) in each scoring volume.

As mentioned previously, however, the main problem of the read-out geometry method requires an additional dedicated-navigator and additional steps to limit the step length within the same scoring volume. Consequently, the read-out geometry method imposes constraints on computational performance.

2.2. Moving voxel-based dose distribution calculator (MVDDC)

We developed a new method called moving voxel-based dose distribution calculator (MVDDC), which is devoted to rapidly calculate a dose distribution in a TM geometry in Geant4. The major problem of calculation of a detailed 3D dose distribution in a TM geometry without using the read-out geometry method is to distribute continuous energy deposition (i.e., $dE_{AlongStep}$) in pertinent scoring volumes. In the majority of the energy range of charged particles used in medical applications, the majority of $dE_{AlongStep}$ consists of ionization of the medium that can be calculated from the stopping power [19]; if we know two parameters, that is, (1) the ratio of a path length included in each scoring volume and a total length of a step and (2) stopping powers at PreStepPoint and PostStepPoint, a $dE_{AlongStep}$ could be distributed in pertinent scoring areas without using the read-out geometry method.

Indeed, the ratio of a path length overlapped on a scoring volume(s) to the total step length can be easily calculated if we know the intersection point(s) between a step ray and a corresponding volume boundary (or boundaries). For this, we newly adopted “moving voxel (MV)” concept in MVDDC. The MV is a pseudo geometry based on *G4Box* class, and it is designed to be moved along with a step in order to calculate the intersection points between a step and the pseudo scoring box. It is worthwhile to note that the MV is not placed in a real (or parallel) world geometry and during this procedure, Geant4 step is not affected by boundaries of the MV. To introduce the basic concept of the MV, let us assume the 2-dimensional (2D) Geant4 simulation with a step in a triangular geometry as Fig. 1(a). The first position of the MV is located taking into account the position information of PreStepPoint of the step and user’s scoring information (e.g., scoring voxel size, the number of scoring voxels, etc.). Subsequently, the MV calculates an intersection point between the step’s path and the voxel boundary (Fig. 1(b)). If the PostStepPoint is not included in the current MV, the MV is moved to the next position with regard to the intersection point and the direction of the step (Fig. 1(c)). These processes are repeated until PostStepPoint is included in the MV. Note that the intersection point can be calculated by using internal functions included in *G4Box* class.

The second parameter, i.e., the stopping powers, can be calculated by using internal functions included in *G4EmCalculator* class.

During a TM simulation based on MVDDC, two deposited energies (i.e., $dE_{AlongStep}$ and $dE_{PostStep}$) are considered in the calculation of dose distribution, the scoring method for the energies is followed as below:

- $dE_{AlongStep}$ is divided by ratios of step lengths and stopping powers and accumulated in each scoring volume with respect to each index calculated by the MV.
- $dE_{PostStep}$ is accumulated in a scoring volume with respect to the index at PostStepPoint.

Fig. 2 shows schematic behaviors of a particle traversing (a) a TM geometry, (b) TM with the read-out geometry, and (c) TM with MVDDC in 2D. In Fig. 2, green and red empty circles mean real step points generated by tetrahedrons and the read-out geometry method, respectively, and a small filled triangle means an intersection point calculated by the MV. As shown in Fig. 2, the read-out geometry generates additional step points (red empty circles), while the MVDDC calculates only intersection points (red filled triangle).

Note that the latest version of Geant4 at the time of this study (i.e., 10.04) has access only to a total deposited energy of a step. For access to $dE_{AlongStep}$ and $dE_{PostStep}$, Geant4 source codes should be modified as shown in Appendix A.

2.3. Evaluation of MVDDC

We performed Geant4 simulations to evaluate the accuracy and performance of the MVDDC. For this evaluation, we assumed that the proton spot beam, which was generated under the same conditions used in a previous study [22], was irradiated to simple TM cubes (size: $200 \times 200 \times 200\,mm^3$) generated by TetGen [23] and the evaluation was performed taking into account various conditions as follows:

1) Number of tetrahedrons: five TM cubes made up of 6, $\sim 10^2$, $\sim 10^3$, $\sim 10^4$, and $\sim 10^5$ tetrahedrons (Fig. 3),
2) Resolution of the scoring voxel: three sizes of scoring voxel ($0.5 \times 0.5 \times 0.5$, $1 \times 1 \times 1$, and $2 \times 2 \times 2\,mm^3$).
3) Energies: three proton beam energies (100, 125, and 150 MeV),
4) Materials: three types of material considering density variation (lung, water, and bone).

It should be noted that to perform the independent evaluation, $\sim 10^3$ tetrahedrons, $1 \times 1 \times 1\,mm^3$ scoring voxel size, 100- MeV proton, and water material were set as the default conditions. The protons beam energies (i.e., 100, 125, and 150 MeV) were considered for the generalization with respect to the G4BetheBlochModel class, which is used for the calculation of the stopping power for charged particles in Geant4. In materials, predefined Geant4 materials (G4_Lung_ICRP, G4_WATER, and G4_BONE_ CORTICAL_ICRP) were used. Note that the density of the lung used was that of an exhaled lung (i.e., $0.495\,g/cm^3$) according to Beardmore et al. [24] instead of originally defined density in G4_Lung_ICRP (i.e., $1.04\,g/cm^3$) considering density difference between lung and water materials.

The evaluations were performed using a server system with 16-core CPUs (Intel® Xeon® CPU E5-2687 W @ 3.10 GHz × 2), 64-GB memory. The version of Geant4 code used in this study was 10.04 patch-01. For the electromagnetic and hadronic physics processes, G4EmLivermorePhysics, G4HadronElasticPhysics, and G4HadronPhysicsFTFP_ BERT_HP physics constructors were used. A cut value of 1 mm was used for the range cut of the secondary particles.

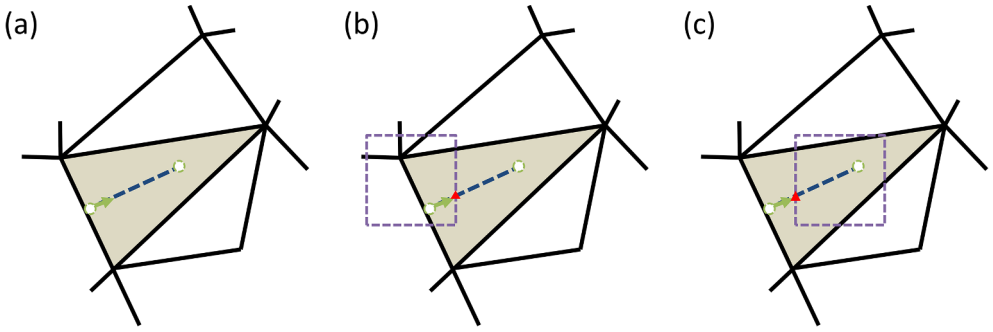

Fig. 1. Schematic procedures of moving voxel (MV, purple dashed line) in a triangle in Geant4: (a) a step occurs, (b) an MV is located at pertinent position taking into account PreStepPoint of the step, and an intersection point (red filled triangle) between the step and the MV's boundary is calculated, and (c) the MV is relocated to the next position. Note that the size of dashed line box represents the scoring voxel size for calculation of dose distribution. (For interpretation of the references to colour in this figure legend, the reader is referred to the web version of this article.)

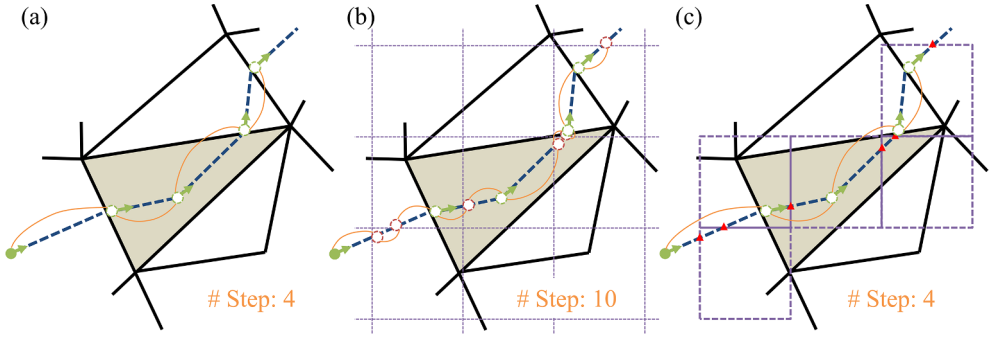

Fig. 2. Comparison of the number of steps in (a) TM geometry, (b) TM and the read-out geometry, and (c) TM and the MVDDC (2D view). Green and red empty circles are real step points generated by tetrahedrons and the read-out geometry method, respectively, and a small filled triangle is an intersection point calculated by the MV. Note that intersection points (red filled triangle) are not related to the number of steps in Geant4. (For interpretation of the references to colour in this figure legend, the reader is referred to the web version of this article.)

2.3.1. Accuracy test

The 3D dose distributions calculated using the MVDDC were compared with those of the TM with the read-out geometry method. In the test, the prepared TM cubes were irradiated with a 10^8 proton spot beam. The gamma index (GI) [25] was used to compare the dose distribution of the calculated MVDDC with that calculated using the read-out geometry method as reference data. The criteria of the GI were set as tightening passing criteria with 1-mm distance-to-agreement (DTA), 1% dose difference (DD), and 10% dose threshold; as an exception, owing to the limited voxel size, a 2-mm DTA was used for the $2 \times 2 \times 2\text{-mm}^3$ size of scoring voxel. The accepted GI passing rate was tightly set as > 95% passed voxels.

2.3.2. Evaluation of computational time

The computational time of MVDDC was measured and compared with that calculated using the read-out geometry method under the same conditions of the previous accuracy test. In this study, conventional simulations of a TM phantom (indicated by "conventional") that scores the absorbed doses in tetrahedrons were performed and their calculation times were also measured to check the increasing ratio of the computational time according to two additional scoring methods. It should be noted that the conventional simulations are meaningless with respect to the 3D dose distribution calculation, and the calculation times of the simulations were simply used in this study as indicators for checking effects of the two additional scoring systems for dose distribution calculation in TM geometry. In this study, the objective of the evaluations is to obtain a measurement of the computational efficiency; hence, only a small number of primary particles was irradiated in all the cases, and the simulation time required for the particle transport excluding the initialization time was only measured. Note that the MVDDC algorithm is only involved in particle transport process when a step algorithm is called, and we internally confirmed that two initialization times with respect to the conventional and MVDDC calculation methods were no significantly different. The performance evaluation was performed in the single-thread mode of Geant4, and each case was repeated more than five times and obtained a statistical uncertainty of less than 5%.

3. Results and discussion

3.1. Accuracy evaluation

From the obtained results, all Gamma Index (GI) passing rates (criteria: 1 mm/1%) of the dose distributions calculated using the MVDDC were higher than 97% as compared with those of the read-out geometry method; that is, the passing rates of GI were sufficiently higher than the tolerance level of 95%. Our results also showed that in additional GI tests with the 1-mm/2% criteria (2-mm/2% criteria for the $2 \times 2 \times 2\text{-mm}^3$ size of scoring voxel as an exception), all the passing rates of GI were higher than 99%. It was thus confirmed that the MVDDC could identically calculate the dose distribution within the statistical uncertainty as compared with that of the read-out geometry method.

Fig. 4 shows the comparison of the dose distributions for a 100-MeV proton spot beam simulation in a TM water cube comprising approximately 10^3 and 10^5 tetrahedrons calculated using the read-out geometry and MVDDC methods.

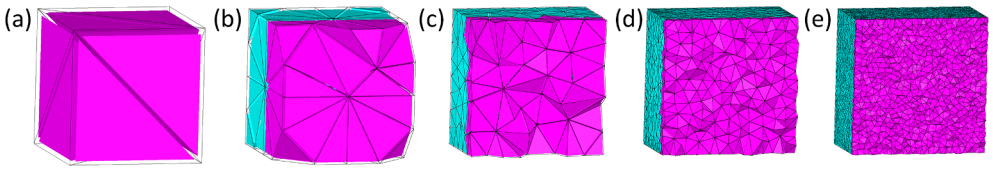

Fig. 3. Cross-sectional views of prepared tetrahedral-mesh cubes comprising (a) six tetrahedrons, (b) ~10^2 tetrahedrons, (c) ~10^3 tetrahedrons, (d) ~10^4 tetrahedrons, and (e) ~10^5 tetrahedrons.

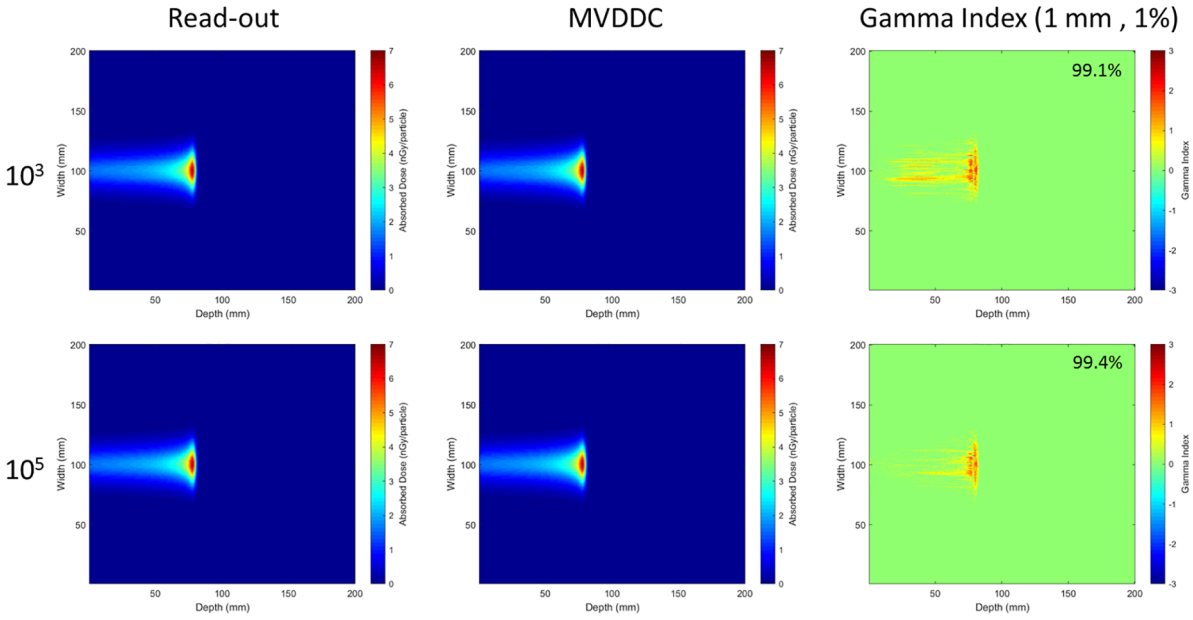

Fig. 4. Comparison of dose distributions for 100-MeV proton spot beam simulation in TM water cube comprising approximately 10^3 (top) and 10^5 (bottom) tetrahedrons calculated using the read-out geometry (left), MVDDC (middle) and gamma index distribution (right). The gamma index passing rates (criteria: 1 mm/1%) was 99.1% and 99.4% respectively.

3.2. Evaluation of calculation speed

3.2.1. Number of tetrahedrons

Table 1 presents the measured computational time required for the TM cube simulations according to the number of tetrahedrons. In the test, the scoring voxel size, energy of the primary proton, and phantom material were set as $1 \times 1 \times 1$ mm^3, 100 MeV, and water, respectively.

The result showed that the calculation speeds of the MVDDC were faster (by factors of 1.7–2.2) than those of the read-out geometry method.

In a comparison with the calculation times of conventional simulation, the increasing ratios of the calculation times obtained using the MVDDC (1.8–2.1) were certainly lower than those obtained for the read-out geometry method (3.0–4.7). The trends of these results can be described as the additional number of steps made by each method. In the read-out geometry method, additional steps were generated by the additional scoring voxel geometry, and the ratio of the additional steps to the total steps was inversely proportional to the number of tetrahedrons that composes the TM cube. In MVDDC, however, the method to calculate dose distribution was not related to the increase in the total number of steps; therefore, it was confirmed that the increasing ratios of the computational time of the MVDDC to those of conventional simulation were fairly constant (near 2.0) regardless of the number of tetrahedrons.

Table 1
Computational times of TM cube in Geant4 according to the number of composed tetrahedrons. In this test, the scoring voxel size, energy of the primary proton, and phantom material were set as $1 \times 1 \times 1$ mm^3, 100 MeV, and water, respectively.

Number of Tetrahedrons	Conventional (A)	Read-out (B)	MVDDC (C)	Increasing ratio (B/A)	Increasing ratio (C/A)	Speed-up factor (B/C)
6	20.7 s	96.8 s	43.9 s	4.7	2.1	2.2
~10^2	22.5 s	99.9 s	46.2 s	4.4	2.0	2.2
~10^3	28.3 s	115.0 s	53.6 s	4.1	1.9	2.1
~10^4	37.9 s	146.2 s	70.6 s	3.9	1.9	2.1
~10^5	55.1 s	162.6 s	98.3 s	3.0	1.8	1.7

3.2.2. Resolution of scoring voxel

Table 2 presents the measured computational time of the TM cube simulations according to the resolution of the scoring voxel. It should be noted that, in this test, the number of tetrahedrons, energy of the primary proton, and phantom material were set as approximately 10^3, 100 MeV, and water, respectively.

In here, the calculation speeds of the MVDDC were faster (by factors of 1.6–3.0) than those of the read-out geometry method.

In a comparison with the calculation times of conventional simulation, the increasing ratios of the calculation times of the MVDDC (1.7–2.2) were lower than those of the read-out geometry method (2.7–6.6). The trends of the results can be explained by almost the same reason as discussed in Section 3.2.1. In the read-out geometry method, the additional steps are strongly related to the increase in the scoring voxel resolution, and the ratio of the additional steps to the total steps was proportional to the number of scoring voxels. However, as previously mentioned, the MVDDC method was not related to the increase in the total number of steps, and therefore, the increasing ratios of the computational time of the MVDDC were fairly constant (near 2.0).

3.2.3. Energy of the primary particle

Table 3 presents the measured computational time for the TM cube simulations according to the energy of the primary proton. It should be noted that, in this test, the number of tetrahedrons, scoring voxel size, and phantom material were set as approximately 10^3, $1 \times 1 \times 1$ mm^3, and water, respectively.

The calculation speeds of the MVDDC were faster (by factors of 2.1–2.7) than those of the read-out geometry method.

In a comparison with the calculation times of conventional simulation, the increasing ratios of the calculation times of the MVDDC (1.9) were lower than those of the read-out geometry method (4.1–5.1). The trends of the results can also be attributed to the same reason as that discussed in Sections 3.2.1 and 3.2.2. In the read-out geometry method, additional steps were generated and the ratio of the additional steps to the total steps was proportional to the primary particle's energy, but in the MVDDC method, the additional steps were not generated.

3.2.4. Material

Table 4 presents the measured computational time for the TM cube

Table 2
Computational times of TM cube in Geant4 according to the resolution of scoring voxel. In this test, the number of tetrahedrons, energy of the primary proton, and phantom material were set as approximately 10^3, 100 MeV, and water, respectively.

Voxel size	Conventional (A)	Read-out (B)	MVDDC (C)	Increasing ratio (B/A)	(C/A)	Speed-up factor (B/C)
$2 \times 2 \times 2\,mm^3$	28.3 s	76.0 s	48.1 s	2.7	1.7	1.6
$1 \times 1 \times 1\,mm^3$	28.3 s	115.0 s	53.6 s	4.1	1.9	2.1
$0.5 \times 0.5 \times 0.5\,mm^3$	28.3 s	187.5 s	62.9 s	6.6	2.2	3.0

Table 3
Computational times of TM cube in Geant4 according to the proton energy. In this test, the number of tetrahedrons, scoring voxel size, and phantom material were set as approximately 10^3, $1 \times 1 \times 1\,mm^3$, and water, respectively.

Energy	Conventional (A)	Read-out (B)	MVDDC (C)	Increasing ratio (B/A)	(C/A)	Speed-up factor (B/C)
100 MeV	28.3 s	115.0 s	53.6 s	4.1	1.9	2.1
125 MeV	35.7 s	162.6 s	69.6 s	4.6	1.9	2.3
150 MeV	44.2 s	224.4 s	83.9 s	5.1	1.9	2.7

Table 4
Computational times of TM cube in Geant4 according to the material. In this test, the number of tetrahedrons, scoring voxel size, and energy of the primary proton were set as approximately 10^3, $1 \times 1 \times 1\,mm^3$, and 100 MeV, respectively.

Material	Conventional (A)	Read-out (B)	MVDDC (C)	Increasing ratio (B/A)	(C/A)	Speed-up factor (B/C)
Lung	48.1 s	266.2 s	130.3 s	5.5	2.7	2.0
Water	28.3 s	120.2 s	53.6 s	4.2	1.9	2.2
Bone	45.7 s	139.7 s	95.2 s	3.1	2.1	1.5

simulations according to the material. It should be noted that, in this test, the number of tetrahedrons, scoring voxel size, and energy of the primary proton were set as approximately 10^3, $1 \times 1 \times 1\,mm^3$, and 100 MeV, respectively.

The results showed that the calculation speeds of the MVDDC were faster (by factors of 1.5–2.2) in all the cases in comparison to those of the read-out geometry method.

In a comparison with the calculation times of conventional simulation, the increasing ratios of the calculation times of the MVDDC (1.9–2.7) were lower than those of the read-out geometry method (3.1–5.5). The results were explained by two factors, (1) a density difference and (2) a complexity of material composition. With respect to the density difference, the results can be explained by the same reason as discussed in Sections 3.2.1 to 3.2.3. because the total number of steps in a simulation with the lung (low density) is larger than that of bone (high density). With respect to the complexity of a material, to the best of the authors' knowledge, the Geant4 navigator requires more time to calculate the physics interaction parameters (e.g., stopping power) in complex composition materials used in this test (i.e., lung and bone) than a simple composition material used in this test (i.e., water).

From the combination of the two factors, the results of the increasing ratio exhibited a slightly different behavior as compared with the previous results; for instance, in the lung, the increasing ratio of the MVDDC calculation times (2.7) was higher than the previous results (near 2.0). Nevertheless, the comprehensive results showed that the computational speeds of the MVDDC were still faster than those of the read-out geometry method.

3.3. Example tests of MVDDC usage for human phantom application

The performances of MVDDC was additionally evaluated for a human phantom application using a THRK-MAN (Yeom et al. 2014) phantom, which is composed of approximately 4×10^5 tetrahedrons and 27 materials. For this study, two simulation cases were considered as follows: (1) 100-MeV proton spot beams irradiated for lung, and (2) 150-MeV proton spot beams irradiated for liver. The performance evaluations were performed under the same conditions of the previous tests, and the scoring voxel size was set as $1 \times 1 \times 1\,mm^3$.

Regarding accuracy test, the GI passing rates (criteria: 1-mm/1%) of the dose distributions calculated using the MVDDC were 99.9% and 98.5% for 100- and 150-MeV proton beams as compared with those of the read-out geometry method, respectively. From the obtained results, it was thus confirmed that the MVDDC could identically calculate the dose distribution within the statistical uncertainty as compared with that of the read-out geometry method.

Table 5 presents the measured computational time of the THRK-MAN simulations. In comparison with the calculation times of conventional simulation, the increasing ratios of the calculation times of the MVDDC were approximately 2.0, which have the same trend as the previous results shown in Section 3.2. However, the increasing ratios of the read-out geometry method presented 2.8–3.0, which were slightly lower than previous results shown in Section 3.2; it is due to the size of tetrahedrons included in THRK-MAN, which is one of the factors with respect to the calculation speed of the read-out geometry method represented in Section 3.2.1. In fact, the increase of the calculation speed of the read-out geometry method was affected by small volumes of tetrahedrons located in very thin organs (e.g., skin, soft tissue) on the way of a beam direction. Nevertheless, the calculation speeds of the MVDDC were still faster (by a factor of 1.4) than those of the read-out geometry method in the real human phantom application.

4. Conclusion

In the present study, a new method, called Moving Voxel-based Dose-Distribution Calculator (MVDDC), was developed to rapidly calculate a 3D dose distribution in a tetrahedral-mesh (TM) geometry which is a very promising geometry for computational human phantoms. The MVDDC estimates the deposited energies using a moving voxel (MV) and stopping powers. To evaluate the performance of the MVDDC, dose distributions in a simple cubic phantom and in a human phantom were calculated using the MVDDC, and the calculated results were compared with those of the simulations using the read-out geometry method. Our results showed that the developed method provides reliable dose distributions, and the usage of the MVDDC improved the computation speed when compared to those of the read-out geometry method for all the cases considered in the present study. For a simple cube, the speed-up factor of the MVDDC was within the range of

Table 5
Computational times of THRK-MAN phantom in Geant4.

Case	Conventional (A)	Read-out (B)	MVDDC (C)	Increasing ratio (B/A)	(C/A)	Speed-up factor (B/C)
Case 1	198.6 s	586.0 s	406.8 s	3.0	2.0	1.4
Case 2	111.8 s	317.0 s	222.9 s	2.8	2.0	1.4

1.5–2.7, depending on the simulation conditions. For a human phantom application, the simulations using the MVDDC were faster by a factor of 1.4 than those of the simulation using the read-out geometry method. The current study presents only the utilization of the MVDDC in a TM geometry, but the MVDDC can also be used to calculate a dose distribution in other unstructured-mesh geometries or constructive solid geometry (CSG) wherein an additional scoring geometry is required for a 3D dose distribution calculation. In addition, the current study presents only the performance of the MVDDC in a single thread; nevertheless, we believe that the MVDDC could be fully utilized in Geant4-MT code because Geant4-MT code was developed based on the event-level parallelism technique, regardless of step calculation algorithm.

Appendix A. . Modification of Geant4 code

Appendix A.1 G4Step.hh file

```
// total energy deposit
G4double GetTotalEnergyDeposit() const;
void SetTotalEnergyDeposit(G4double value);
// [USER ADDED] energy deposit for AlongStep and PostStep
G4double GetEnergyDepositForAlongStep() const;
G4double GetEnergyDepositForPostStep() const;
void SetEnergyDepositForAlongStep();
void SetEnergyDepositForPostStep();
// total non-ionizing energy deposit
G4double GetNonIonizingEnergyDeposit() const;
void SetNonIonizingEnergyDeposit(G4double value);
.
.
.
[SKIP a few lines]
.
.
.
//————————————————
protected:
//————————————————
// Member data
G4double fTotalEnergyDeposit;
// Accummulated total energy desposit in the current Step
// [USER ADDED] energy deposit for AlongStep and PostStep
G4double fEnergyDepositForAlongStep;
G4double fEnergyDepositForPostStep;
G4double fNonIonizingEnergyDeposit;
// Accummulated non-ionizing energy desposit in the current Step
```

Appendix A.2 G4Step.icc file

```
inline
void G4Step::SetTotalEnergyDeposit(G4double value)
{
  fTotalEnergyDeposit = value;
}
// [USER ADDED] Definition of Get and Set functions
// for dE_AlongStep and dE_PostStep
inline
G4double G4Step::GetEnergyDepositForAlongStep() const
{
  return fEnergyDepositForAlongStep;
}
inline
G4double G4Step::GetEnergyDepositForPostStep() const
{
  return fEnergyDepositForPostStep;
}
inline
void G4Step::SetEnergyDepositForAlongStep()
{
  fEnergyDepositForAlongStep = fTotalEnergyDeposit;
}
inline
void G4Step::SetEnergyDepositForPostStep()
{
  fEnergyDepositForPostStep
   = fTotalEnergyDeposit - fEnergyDepositForAlongStep;
}
inline
```

Acknowledgements

This project was supported by the Nuclear Safety Research and Development (NSR&D) Program through the Korea Foundation of Nuclear Safety (KoFONS) and funded by the Nuclear Safety and Security Commission (NSSC) and by Basic Science Research Program through the National Research Foundation of Korea (NRF) funded by the Ministry of Education (Project Nos.: 1705006, 2016R1D1A1A-09916337). One of the authors (Haegin Han) was supported by the Global PhD Fellowship program (Project No.: NRF-2018H1A2A1059767).

```
G4double G4Step::GetNonIonizingEnergyDeposit() const
{
  return fNonIonizingEnergyDeposit;
}
```

Appendix A.3 G4SteppingManager.cc file

```
  // Update safety after invocation of all AlongStepDoIts
  endpointSafOrigin = fPostStepPoint- > GetPosition();
  endpointSafety = std::max(proposedSafety - GeomStepLength, kCarTolerance);
  fStep- > GetPostStepPoint()- > SetSafety(endpointSafety);
  // [USER ADDED] energy deposit for alongStep
  fStep- > SetEnergyDepositForAlongStep();
#ifdef G4VERBOSE // !!!!! Verbose
  if(verboseLevel > 0) fVerbose- > AlongStepDoItAllDone();
#endif
  // Invoke PostStepDoIt
  InvokePostStepDoItProcs();
  // [USER ADDED] energy deposit for postStep
  fStep- > SetEnergyDepositForPostStep();
#ifdef G4VERBOSE // !!!!! Verbose
  if(verboseLevel > 0) fVerbose- > PostStepDoItAllDone();
#endif
}
```

References

[1] Giacometti V, Guatelli S, Bazalova-Carter M, Rosenfeld AB, Schulte RW. Development of a high resolution voxelised head phantom for medical physics applications. Phys Med 2017;33:182–8.

[2] Papadimitroulas P. Dosimetry applications in GATE Monte Carlo toolkit. Phys Med 2017;41:136–40.

[3] Zvereva A, Schlattl H, Zankl M, Becker J, Petoussi-Henss N, Yeom YS, et al. Feasibility of reducing differences in estimated doses in nuclear medicine between a patient-specific and a reference phantom. Phys Med 2017;39:100–12.

[4] Kim CH, Jeong JH, Bolch WE, Cho KW, Hwang SB. A polygon-surface reference Korean male phantom (PSRK-Man) and its direct implementation in Geant4 Monte Carlo simulation. Phys Med Biol 2011;56:3137–61.

[5] Bert J, Lemarechal Y, Visvikis D. New hybrid voxelized/analytical primitive in Monte Carlo simulations for medical applications. Phys Med Biol 2016;61:3347–64.

[6] Lee C, Lodwick D, Hasenauer D, Williams JL, Lee C, Bolch WE. Hybrid computational phantoms of the male and female newborn patient: NURBS-based whole-body models. Phys Med Biol 2007;52:3309–33.

[7] Xu XG, Taranenko V, Zhang J, Shi C. A boundary-representation method for designing whole-body radiation dosimetry models: pregnant females at the ends of three gestational periods–RPI-P3, -P6 and -P9. Phys Med Biol 2007;52:7023–44.

[8] Zhang J, Na YH, Caracappa PF, Xu XG. RPI-AM and RPI-AF, a pair of mesh-based, size-adjustable adult male and female computational phantoms using ICRP-89 parameters and their calculations for organ doses from monoenergetic photon beams. Phys Med Biol 2009;54:5885–908.

[9] Yeom YS, Jeong JH, Han MC, Kim CH. Tetrahedral-mesh-based computational human phantom for fast Monte Carlo dose calculations. Phys Med Biol 2014;59:3173–85.

[10] Dukov N, Bliznakova K, Feradov F, Ridlev I, Bosmans H, Mettivier G, et al. Models of breast lesions based on three-dimensional X-ray breast images. Phys Med 2019;57:80–7.

[11] Sarno A, Mettivier G, Di Lillo F, Bliznakova K, Sechopoulos I, Russo P. Homogeneous vs. patient specific breast models for Monte Carlo evaluation of mean glandular dose in mammography. Phys Med 2018;51:56–63.

[12] Sarno A, Mettivier G, Di Lillo F, Tucciariello RM, Bliznakova K, Russo P. Normalized glandular dose coefficients in mammography, digital breast tomosynthesis and dedicated breast CT. Phys Med 2018;55:142–8.

[13] Bliznakova K, Dukov N, Feradov F, Gospodinova G, Bliznakov Z, Russo P, et al. Development of breast lesions models database. Phys Med 2019. in press.

[14] Nguyen TT, Yeom YS, Kim HS, Wang ZJ, Han MC, Kim CH, et al. Incorporation of detailed eye model into polygon-mesh versions of ICRP-110 reference phantoms. Phys Med Biol 2015;60:8695–707.

[15] Yeom YS, Kim HS, Nguyen TT, Choi C, Han MC, Kim CH, et al. New small-intestine modeling method for surface-based computational human phantoms. J Radiol Prot 2016;36:230–45.

[16] Kim CH, Yeom YS, Nguyen TT, Han MC, Choi C, Lee H, et al. New mesh-type phantoms and their dosimetric applications, including emergencies. Ann ICRP 2018;47:45–62.

[17] Agostinelli S, Allison J, Amako K, Apostolakis J, Araujo H, Arce P, et al. GEANT4-a simulation toolkit. Nucl Instrum Meth A 2003;506:250–303.

[18] Allison J, Amako K, Apostolakis J, Araujo H, Dubois PA, Asai M, et al. Geant4 developments and applications. IEEE T Nucl Sci 2006;53:270–8.

[19] Allison J, Amako K, Apostolakis J, Arce P, Asai M, Aso T, et al. Recent developments in GEANT4. Nucl Instrum Meth A 2016;835:186–225.

[20] Geant4 User's Guide for Application Developers 2012 (Geneva: Geant4 Publications).

[21] Sarrut D, Bardies M, Boussion N, Freud N, Jan S, Letang JM, et al. A review of the use and potential of the GATE Monte Carlo simulation code for radiation therapy and dosimetry applications. Med Phys 2014;41.

[22] Seo J, Han MC, Yeom YS, Lee HS, Kim CH, Jeong JH, et al. Temporal resolution required for accurate evaluation of the interplay effect in spot scanning proton therapy. J Korean Phys Soc 2017;70:720–5.

[23] Si H. TetGen, a Delaunay-based quality tetrahedral mesh generator. Acm T Math Software 2015;41.

[24] Beardmore AB, Rosen II, Cheek DA, Fields RS, Hogstrom KR. Evaluation of MVCT images with skin collimation for electron beam treatment planning. J Appl Clin Med Phys 2008;9:2773.

[25] Low DA, Harms WB, Mutic S, Purdy JA. A technique for the quantitative evaluation of dose distributions. Med Phys 1998;25:656–61.